Provided for non-commercial research and education use.
Not for reproduction, distribution or commercial use.

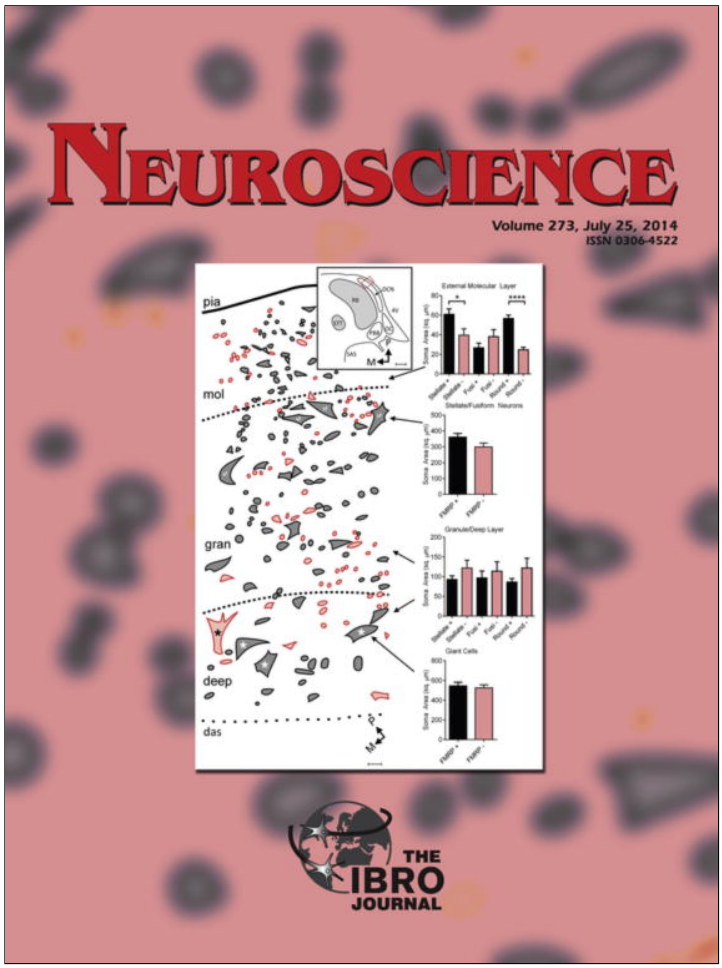

This article appeared in a journal published by Elsevier. The attached copy is furnished to the author for internal non-commercial research and education use, including for instruction at the authors institution and sharing with colleagues.

Other uses, including reproduction and distribution, or selling or licensing copies, or posting to personal, institutional or third party websites are prohibited.

In most cases authors are permitted to post their version of the article (e.g. in Word or Tex form) to their personal website or institutional repository. Authors requiring further information regarding Elsevier's archiving and manuscript policies are encouraged to visit:

http://www.elsevier.com/authorsrights

Author's personal copy

Neuroscience 273 (2014) 79–91

DISTRIBUTION OF FRAGILE X MENTAL RETARDATION PROTEIN IN THE HUMAN AUDITORY BRAINSTEM

K. BEEBE, [a] **Y. WANG** [b] **AND R. KULESZA** [a]*

[a] *Lake Erie College of Osteopathic Medicine, Auditory Research Center, Erie, PA, USA*

[b] *Virginia Merrill Bloedel Hearing Research Center, Department of Otolaryngology-Head and Neck Surgery, University of Washington School of Medicine, Seattle, WA, USA*

Abstract—Fragile X mental retardation protein (FMRP) binds select mRNAs, functions in intracellular transport of these mRNAs and represses their translation. FMRP is highly expressed in neurons and lack of FMRP has been shown to result in dendritic dysmorphology and altered synaptic function. FMRP is known to interact with mRNAs for the Kv3.1b potassium channel which is required for neurons to fire action potentials at high rates with remarkable temporal precision. Auditory brainstem neurons are known for remarkably high spike rates and expression of Kv3.1b potassium channels. Fragile X syndrome (FXS) is a genetic disorder caused by a mutation in the fragile X mental retardation 1 gene (Fmr1) resulting in decreased expression of FMRP and subsequent intellectual disability, seizures, attention deficit and hypersensitivity to auditory and other sensory stimuli. We therefore hypothesize that the auditory difficulties in FXS result, at least in part, from dysfunction of auditory brainstem neurons. To examine this hypothesis, we have studied normal human brainstem tissue with immunohistochemical techniques and confocal microscopy. Our results demonstrate that FMRP is widely expressed in cell bodies and dendritic arbors of neurons in the human cochlear nucleus and superior olivary complex and also that coincidence detector neurons of the medial superior olive colocalization of FMRP and Kv3.1b. We interpret these observations to suggest that the lower auditory brainstem is a potential site of dysfunction in FXS.
© 2014 IBRO. Published by Elsevier Ltd. All rights reserved.

Key words: hearing, cochlear nucleus, superior olive.

INTRODUCTION

Fragile X mental retardation protein (FMRP) is the product of the Fmr1 gene and is widely expressed in multiple tissues from the embryonic period into adulthood (Hinds et al., 1993). FMRP is an RNA-binding protein that functions mainly in activity-dependent translational regulation of a large number of mRNAs, including Kv3.1b and slack potassium channels, and is found both pre and post-synaptically (Akins et al., 2009, 2012; Strumbos et al., 2010; Zhang et al., 2012). Although, translation-independent actions of FMRP have recently been discovered (Brown et al., 2010; Zhang et al., 2012; Deng et al., 2013). In the adult, FMRP is widely expressed in epithelia [e.g. seminiferous tubules of the testis; esophagus] and nervous tissue (Hinds et al., 1993). In the brain, FMRP is expressed in neurons and glia throughout the brainstem, forebrain and cerebellum (Hinds et al., 1993; Feng et al., 1997; Wang et al., 2004; Jacobs et al., 2012), although not ubiquitously (Devys et al., 1993).

Fragile X syndrome (FXS) is the most common inherited form of intellectual disability (Bassell and Warren, 2008) and results from a CGG triplet repeat expansion in the Fmr1 gene (Verkerk et al., 1991) and consequent repression of FMRP. FXS affects 1:3600 males and 1:8000 females (Cornish et al., 2008), is the most common genetic cause of autism (Bassell and Warren, 2008) and 15–30% of all FXS patients demonstrate autistic behaviors (Rogers et al., 2001; Hatton et al., 2006; Harris, 2011). Patients with FXS display cognitive disabilities, social deficits including language delays, seizures, autistic features, sensory hypersensitivity and hyperactivity (Eliez et al., 2001; Berry-Kravis, 2002; Hagerman et al., 2009). FXS is associated with a number of CNS dysmorphologies, including reduced volume of the cerebellar vermis, enlargement of the 4th ventricle (Mostofsky et al., 1998; Hoeft et al., 2010) and hypertrophy of the hippocampus (Kates et al., 1997) and caudate nucleus (Reiss et al., 1995; Eliez et al., 2001; Hoeft et al., 2010). Alterations in synaptic structure and function have been identified in FXS patients and animal models of FXS (e.g. Fmr1 knockouts [Fmr1 KO]; Pfeiffer and Huber, 2009) and a number of presynaptic and postsynaptic proteins have abnormal levels in Fmr1 KO (Li et al., 2002; Klemmer et al., 2011). Furthermore, in FXS and Fmr1 KO there is a high density of immature dendritic spines (human – Rudelli et al., 1985; Hinton et al., 1991; Comery et al., 1997; Irwin et al., 2000; mouse – Nimchinsky et al., 2001; Galvez et al., 2003). Cultured

*Corresponding author. Address: Lake Erie College of Osteopathic Medicine, Auditory Research Center, Erie, PA 16509, USA. Tel: +1-814-866-8423.
E-mail address: rkulesza@lecom.edu (R. Kulesza).

Abbreviations: AbN, abducens nucleus; cVCN, caudal ventral cochlear nucleus; DCN, dorsal cochlear nucleus; FMR1/Fmr1, fragile X mental retardation 1 gene; Fmr1 KO, Fmr1 knockouts; FMRP, fragile X mental retardation protein; FMRP+, FMRP positive; FN, facial nucleus; FXS, fragile X syndrome; GBC, globular bushy cell; IO, principal nucleus of the inferior olive; ITDs, interaural time differences; LNTB, lateral nucleus of the trapezoid body; LSO, lateral superior olive; MNTB, medial nucleus of the trapezoid body; MSO, medial superior olive; NDS, normal donkey serum; OC, octopus cell region; PB, sodium phosphate buffer; PN, pontine nuclei; SBC, spherical bushy cell; SOC, superior olivary complex; SPON, superior paraolivary nucleus; TBS, Tris-buffered saline; VCN, ventral cochlear nucleus.

http://dx.doi.org/10.1016/j.neuroscience.2014.05.006
0306-4522/© 2014 IBRO. Published by Elsevier Ltd. All rights reserved.

Author's personal copy

hippocampal neurons from Fmr1 KO mice give rise to shorter dendrites with fewer dendritic spines compared to controls (Braun and Segal, 2000; Castren et al., 2005) and FMRP-deficient mice have abnormally arranged dendritic fields in the somatosensory cortex (Galvez et al., 2003), more primary dendrites in the olfactory bulbs (Galvez et al., 2005) and spinal motor neurons with immature dendritic arbors (Thomas et al., 2008). Fmr1 KO flies also demonstrate significant overgrowth of dendrites and axons (Zarnescu et al., 2005). These results, taken together, suggest that FMRP plays a role essential to normal maturation and function of the central nervous system.

In our previous post-mortem studies of the autistic brain, we examined the brainstem of a 32-year-old male diagnosed with autism and FXS (Kulesza and Mangunay, 2008). In this case, we observed neurons in the medial superior olive (MSO), a prominent brainstem nucleus which contains coincidence detector neurons that function in sound source localization and encoding temporal features of sound, to be significantly smaller (a nearly 50% reduction in cell body area) and significantly more round (i.e. immature) compared to an age-matched control (Kulesza and Mangunay, 2008). Moreover, there was significantly more variability in the orientation of these MSO neurons in the FXS/autism brain compared to an age-matched control. In addition, we have demonstrated that FMRP is highly expressed in brainstem coincidence detector neurons across species including the nucleus laminaris of alligator and chicken and the MSO in gerbils and human (Wang et al., 2013). Together, we interpret the dysmorphology of MSO neurons in FXS and the abundance of FMRP in the MSO to suggest that auditory-processing deficits in FXS result, at least in part, from dysfunction of brainstem centers. Further, it is believed that the cell types which express FMRP are the most severely impacted in FXS (Hinds et al., 1993) and we hypothesize that FMRP is widely expressed in neuronal cell bodies and dendritic arbors in the cochlear nuclei and superior olivary complex (SOC). Additionally, FMRP is known to play an important role in activity-dependent regulation and tonotopic expression of the Kv3.1b potassium channel in the auditory brainstem and the tonotopic gradient of Kv3.1b expression is required for accurate coding of complex sounds (Strumbos et al., 2010). To examine the distribution of FMRP in the human auditory brainstem and explore possible functional deficits in FXS, we have used immunohistochemistry and confocal microscopy to map the distribution of FMRP in control human dorsal and ventral cochlear nuclei (DCN and VCN) and SOC. Furthermore, we have examined the colocalization of FMRP and Kv3.1b in the MSO.

EXPERIMENTAL PROCEDURES

Tissue sectioning

This report is based on the examination of brainstems from seven individuals ranging in age from 57 to 96 years of age (average 78.6 ± 5.9 years; five female/two male). Table 1 shows the age, cause of death and post-mortem interval for specimens used in this study. All specimens were obtained with permission from the PA Humanities Gifts Registry. Brainstems were only included in this study if they met the following criteria: (1) the cause of death was not neurological, (2) there were no signs of degenerative disease affecting the brain on gross examination or sectioning, (3) there were no signs of pathology affecting the brainstem or posterior cranial fossa and (4) the brainstems could be preserved within 24-h of death. Brains were dissected immediately from the skull, bisected and placed in cold fixative (4% paraformaldehyde in 0.1 M sodium phosphate buffer [PB], pH 7.2) for at least 2 weeks. Before sectioning, brainstems were trimmed and placed into a solution of 30% sucrose in the same fixative until they were saturated (at least 1 week). Tissue blocks including the cochlear nucleus and superior olive were sectioned on a freezing microtome at a thickness of 40 μm and collected in 0.1 M PB. An ordered series of sections was reserved for Giemsa staining (as previously described – Kulesza, 2007, 2008) and utilized for landmarking purposes.

Antisera

FMRP. Rabbit anti-FMRP polyclonal antibody (ab17722, Abcam, Cambridge, MA) was raised against a synthetic peptide conjugated to KLH derived from within residues 550 to the C-terminus of human FMRP and is known to react with mouse, rat and human FMRP. This antibody identifies 75 and 80-kDa bands on Western blot (Abcam datasheet) and endogenous FMRP is expected to be a 71-kDa band. The difference in band size may be related to known post-translational modifications of FMRP. This antibody has been further characterized by Western blot analysis and immunohistochemistry in mouse, rat and gerbil where bands of ~80 and 70-kDa are identified (Wang et al., 2013).

Kv3.1b. Mouse anti-Kv3.1b monoclonal antibody (NeuroMab, Davis, CA) was raised against a fusion protein of amino acids 437–585 (C-terminus) of rat Kv3.1b. This antigen shares 100% identity with mouse and human Kv3.1b. This antibody identifies a band of 110-kDa on Western blot.

Immunohistochemistry

Free-floating tissue sections were rinsed in 0.1 M PB, endogenous peroxidase activity was quenched with a 10-min wash in 1.5% hydrogen peroxide in PB and tissue was permeabilized in 0.5% Triton X100 in PB. Sections were blocked in 0.1% normal donkey serum (NDS) and incubated overnight in 1% NDS and anti-FMRP antisera (1:750–1000). Tissue sections were rinsed in PB and incubated in biotinylated goat anti-rabbit secondary (1:100; Vector Labs, Inc., Burlingame, CA) for 2-h, rinsed and incubated in ABC solution (Vector Labs) for 1 h. Tissue sections were again washed in PB and then Tris-buffered saline (TBS; pH 7.7) and the final peroxidase reaction was developed in TBS with 0.05% diaminobenzidine, 0.125% nickel ammonium sulfate and 0.06% hydrogen peroxide.

Author's personal copy

Table 1. Specimens with FMRP immunohistochemistry

Specimen #	Age	Sex	Cause of death	PMI (h)
2010.01	57	M	Respiratory failure, sepsis, cardiac	< 24
2011.62	82	F	Atrial fibrillations	< 18
2011.63	84	F	Metastatic breast cancer	< 5
2011.64	77	F	Diabetes/chronic renal disease	< 8
2011.65	95	F	COPD	< 5
2012.16	96	F	Melanoma	< 24
2012.22	59	M	Lung cancer	< 5

Finally, tissue sections were rinsed in TBS, mounted onto glass slides, dried and coverslipped with permount (Fisher Scientific, Inc., Pittsburgh, PA). An alternating series of sections was counterstained with neutral red, dehydrated, cleared and coverslipped. Tissue sections processed without addition of the primary antibody revealed no reaction product.

Analysis

Neurons in the cochlear nucleus and SOC were reconstructed as closed contours using a drawing tube attached to an Olympus BX45 microscope; tracings were digitized, imported into ImageJ and calibrated to a standard scale bar. Neuronal morphology was characterized using the "measure" feature in ImageJ. Cellular profiles were classified as immunopositive if they contained dark brown/black DAB reaction product. Cell bodies were classified as immunonegative if they only contained neutral red stain. For counting purposes and our analyses of cell body size and shape, we employed a uniform, random sampling strategy to include cell bodies from the rostral–caudal length of the cochlear nuclei and SOC. The proportion of immunopositive somata was determined by comparing the number of immunpositive somata with the total number of neurons (total = immunopositive + neutral red only) within a nucleus/region. Cell body profiles were traced using a Camera Lucida attachment (Olympus) while focusing to produce clear somatic contours. Tracings were digitized and analyzed with ImageJ software (calibrated to a standard scale bar [final on-paper magnification of 1000×]; available at http://rsb.info.nih.gov/ij). An index of circularity was calculated as previously described (Yin and chan, 1990; Kulesza, 2007). All data sets were tested for a normal distribution using the D'Agostino & Pearson omnibus test; if a normal distribution was met, data were compared using parametric tests (*t*-tests, analysis of variance (ANOVA)). Data that failed to meet a normal distribution were compared using nonparametric tests (i.e. Mann–Whitney or Kruskal–Wallis with Dunn post hoc test). All statistical analyses were made in Prism 6 (GraphPad Software) with a 0.05 significance level.

The location of MSO neurons (FMRP+ and FMRP−) was mapped from the middle (rostrocaudal) 1/3 of the nucleus by tracing cell body profiles within the borders of the MSO. Tracings were normalized (i.e. rotated to fit a vertical contour and cropped to only include the MSO) and imported into ImageJ. The posterior tip of the MSO was set to "0" along the *Y*-axis and the medial border was set to "0" along the *X*-axis. The medial–lateral and anterior–posterior location was determined by measuring the "centroid" (*X* and *Y* coordinates) of each neuron using the "measure" feature in ImageJ.

Immunofluorescence

Tissue was sectioned as described above and free-floating sections were rinsed in PB and permeablized for 2-h in a solution of 0.5% Triton X100 and 1% NDS. Tissue sections were incubated overnight in a solution of rabbit anti-FMRP (1:500; Abcam, ab17722) and mouse anti-Kv3.1b (1:500; NeuroMab), rinsed in PB and incubated for at least 2-h in a cocktail of DyLight 488 anti-rabbit (Vector Labs; 1:100) and DyLight 549 anti-mouse (Vector Labs; 1:100). Tissue sections were then mounted onto glass slides from PB and coverslipped with Vectashield hard set fluorescent mounting media (Vector Labs) and viewed on a Leica TCS SP 5 confocal microscope using the LAS AF program.

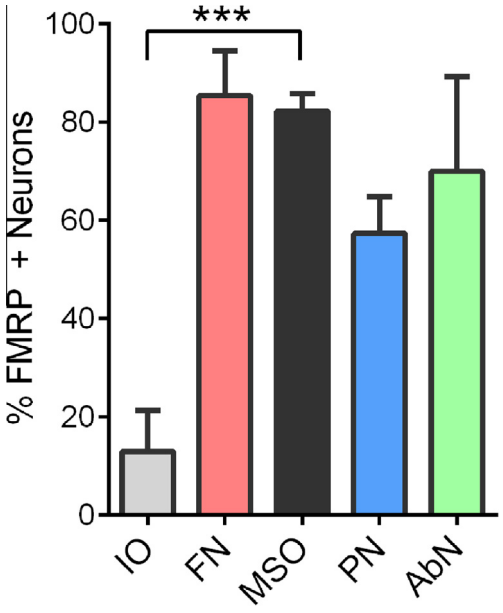

Fig. 1. Differential expression of FMRP in brainstem neurons. The number of FMRP+ neurons is demonstrated for various nuclei within the human brainstem. Approximately 78% of all human MSO neurons were FMRP+. The human facial nucleus (FN) included significantly more FMRP+ neurons (nearly 87%). However, the pontine nuclei (PN), the abducens nucleus (AbN) and the principle nucleus of the inferior olive (IO) had fewer FMRP+ neurons (58%, 69% and 14%, respectively).

Author's personal copy

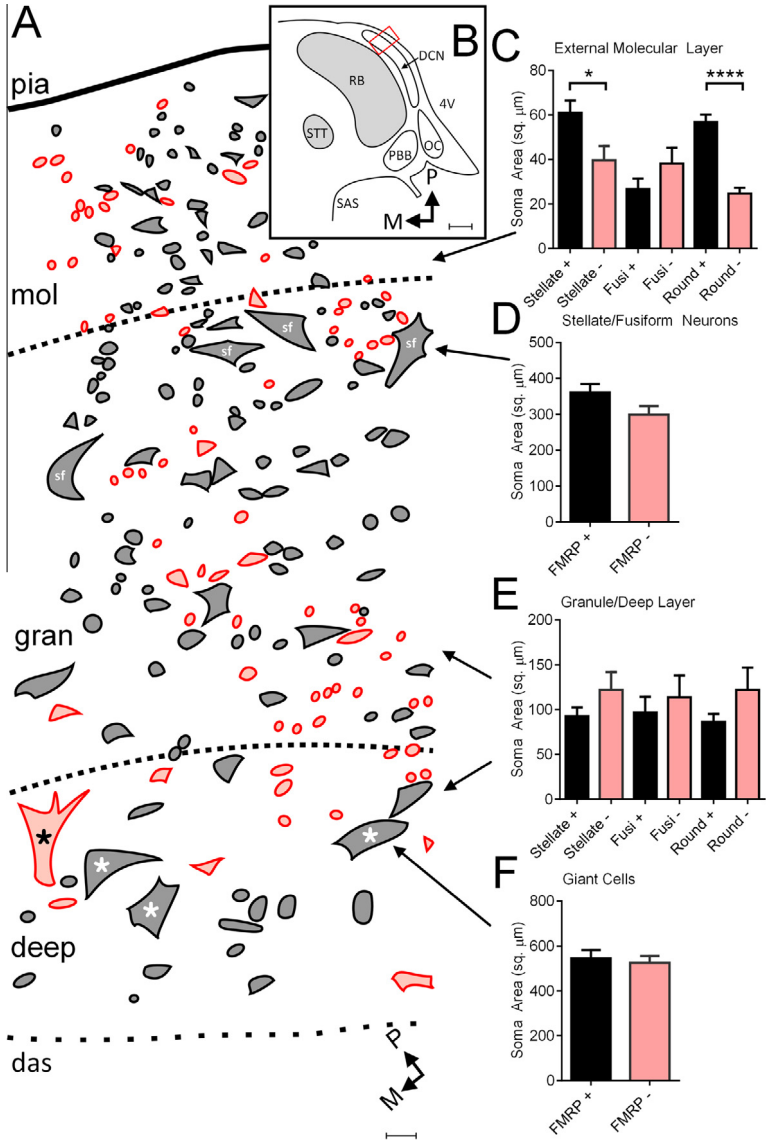

Fig. 2. FMRP is widely expressed in the human DCN. A demonstrates a rectangular segment of the human DCN from the posterior aspect of the nucleus; the rectangle in B indicates schematically the location of the illustrated segment. In A, all neuronal contours were traced and coded according to FMRP-immunoreactivity (black = FMRP+; red = FMRP-immunonegative). Shown in C–F are plots of cell types, cell body size by FMRP-immunoreactivity. In the molecular layer (mol), FMRP+ stellate neurons had significantly larger somata than FMRP-immunonegative stellate neurons. At the interface between the molecular and granule layer (gran) was a population of large stellate/fusiform neurons (sf). In the deepest part of the DCN there was (among other smaller neuronal profiles) a population of giant cells (asterisks in A). Scale bar = 20 µm (A) and Scale bar = 1 mm (B). (For interpretation of the references to color in this figure legend, the reader is referred to the web version of this article.)

Examination of tissue sections processed for immunofluorescence without primary antisera revealed only lipofuscin artifacts (see Fig. 8).

Anatomical subdivisions and terminology

According to our previous description (Wagoner and Kulesza, 2009), we divided the DCN into three layers: an external molecular layer, a granule layer and a deep layer. For our analyses, we condensed the granule and deep layers, but examined separately the larger stellate/fusiform cells found at the molecular/granule layer interface and the giant cells found in the deep layer. In the DCN, there is a substantial population of small, round cells and we found it difficult to distinguish with certainly which of these cells were granule cells and which were glia. Therefore, we avoided analysis of this population of small, round cells. Terminology for neuronal subtypes in the human VCN used herein is based on those established by Osen, 1969; Moore and Osen, 1979) and recent descriptions of these cell types (Wagoner and Kulesza, 2009; Kulesza, 2013). VCN neurons were characterized according to cell body morphology, primary dendrites and location within the VCN. The classification scheme for SOC nuclei is based on previous work from this lab (Kulesza, 2007, 2008; Schmidt et al., 2010; Kulesza et al., 2011; Kulesza, 2013). Finally, we have employed terminology conventionally used for human neuroanatomical imaging (Standring, 2008). Thus, caudal indicates toward the spinal cord, rostral indicates toward the

Author's personal copy

midbrain, posterior (dorsal) indicates toward the back of the head and anterior (ventral) indicates toward the face. For obvious reasons, we will avoid the terms ''anteroventral'' or ''posteroventral'' to describe the human cochlear nuclei.

RESULTS

General brainstem distributions

In order to obtain a more global understanding of the neuronal distribution of FMRP in the human brainstem, we estimated the number of FMRP+ neurons in nuclei along the rostro-caudal length of the brainstem. Specifically, we examined FMRP expression in the principal nucleus of the inferior olive (IO), facial nucleus (FN), MSO, pontine nuclei (PN) and the abducens nucleus (AbN). We found that the vast majority of neurons in the FN and MSO were FMRP+ (Fig. 1; 85 ± 9% and 82 ± 9%, respectively; mean ± standard deviation). However, we found that 57 ± 6% of neurons in the PN and 70 ± 15% of neurons in the AbN were FMRP+, but only 13 ± 9% of neurons in the IO were FMRP+. Relative to the MSO, the IO contained significantly fewer FMRP+ neurons (Fig. 1; Kruskal–Wallis, $p < .005$; Dunn's test for multiple comparisons).

Cochlear nucleus

Overall, we found that FMRP was widely expressed in human cochlear nucleus neurons. In the dorsal cochlear nucleus (DCN) the majority of neurons were FMRP+ but this varied by layer and cell type (Fig. 2). The external molecular layer (mol) was composed mainly of axons (Wagoner and Kulesza, 2009), although there was a sparse population of small neurons (Fig. 2A). The neurons within the molecular layer were dominated by small round cells (73% of total), but there are also small stellate neurons (24% of total) and few small fusiform neurons (4%; Fig. 2A). In the molecular layer, the majority of neurons were FMRP+ (Fig. 2C; 66% of round, 74% of stellate and 43% of fusiform). In this layer, FMRP+ cells were generally larger than FMRP–immunonegative cells (round = 57 ± 3 μm^2 vs. 25 ± 3 μm^2 [$p < .0001$]; stellate = 61 ± 6 μm^2 vs. 40 ± 6 μm^2, t-test, $p = .02$). At the interface between the molecular and granule layers there was a population of large stellate/fusiform neurons often found in clusters of 2–4 (Fig. 2A, sf). These neurons had an average cell body area of 361 ± 24 μm^2 and 91% was FMRP+. Deep within the molecular layer there was a band containing a high density of neuronal cell bodies with many small, round cell bodies. Deep within this granule layer (Fig. 2A, gran) was a so-called deep layer which had a relatively low density of neuronal cell bodies but includes the somata of giant cells (Fig. 2A, asterisks). The granule and deep layers were dominated by small round/oval cells (51% of total, excluding large stellate/fusiform and giants cells). Small stellate neurons made up 29% of the total and small fusiform neurons made up 19% of the total neuronal population in this layer. The majority (83%) of small round cells were FMRP+. Although we could not with certainty eliminate glial cells from our analysis, we observed a trend for FMRP–immunonegative round cells to be larger than FMRP+ cells in this layer (Fig. 2E; 122 ± 24 vs. 86 ± 9 μm^2) although the number was too small for statistical comparisons. Additionally, the majority of small stellate (78%) and fusiform cells (60%) were FMRP+ and we found no significant difference in the cell bodies size between FMRP+ and FMRP-immunonegative populations (2E). Finally, within the deep layer there was a population of giant cells with stellate or pyramidal morphology (Fig. 2A, asterisks). Giant cell somata averaged 536 ± 24 μm^2, 53% of which were FMRP+. We found no statistical difference in cell body size between FMRP+ and FMRP-immunonegative

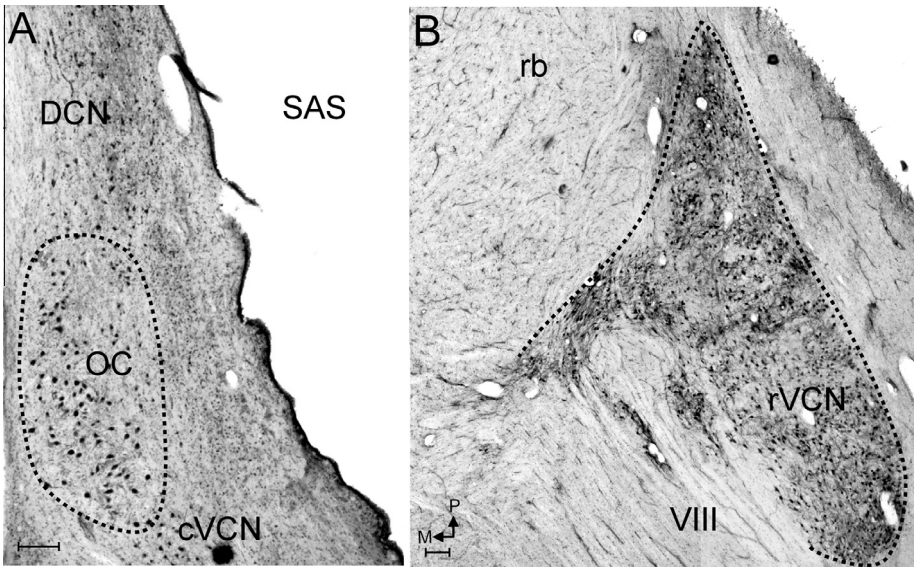

Fig. 3. FMRP is widely expressed in the VCN. Shown in A is the caudal pole of the VCN; the octopus cell region is indicated by the dashed line. The majority of octopus cells and stellate cells in this region are FMRP+. A more rostral level through the VCN and vestibulocochlear nerve (VIII) is shown in B. At this level, the GBC are evident near the nerve root while SBC and stellate neurons are found more posteriorly. Scale bar = 200 μm.

Author's personal copy

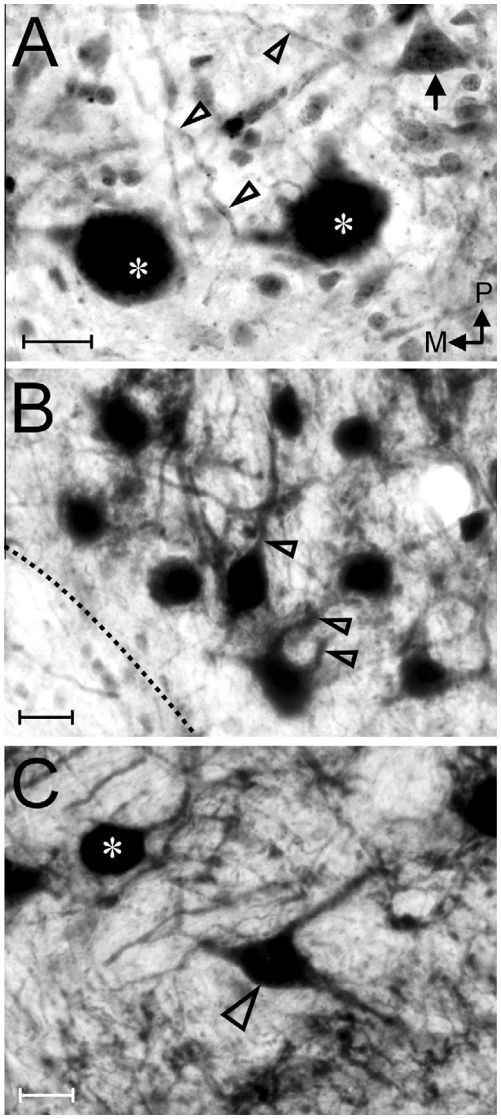

Fig. 4. Most VCN cell types are FMRP+. Shown in A are examples of FMRP+ octopus cells and an FMRP-immunonegative stellate neuron (neutral red stain; arrow). Numerous thin FMRP+ profiles are found traversing the octopus cells region (presumed axons; arrowheads). Shown in B are examples of FMRP+ GBC; dendritic profiles are indicated by arrowheads. Shown in C are examples of FMRP+ SBC (asterisk) and a large stellate neuron (arrowhead). Scale bar = 20 μm.

giant cell populations (2F; 545 ± 37 vs. 526 ± 31 μm^2; *t* test, $p = .69$).

In the VCN the majority of neurons were FMRP+ but again this varied by region and cell type. In the caudal VCN (cVCN; Fig. 3A) there was a collection of octopus cells (OC; Fig. 4A, asterisks) intermingled with stellate neurons (Fig. 4A, arrow). The vast majority of octopus cells were FMRP+ (89%, Fig. 5) and FMRP+ octopus cells had significantly larger somata compared to FMRP-immunonegative octopus cells (466 ± 15 μm^2 compared to 370 ± 21 μm^2; Mann–Whitney, $p = .01$, Fig. 5C). FMRP-immunolabeling was not restricted to octopus cell somata and FMRP+ dendritic profiles emerged from FMRP+ somata. Additionally, there were numerous thin, FMRP+ fibers, which we interpreted as axonal profiles, coursing through the octopus cell region (OC) and these axons appeared to course in a predominately anterior–posterior direction (Fig. 4A, arrowheads).

Rostral to the OC, at the level of the entering auditory nerve, the vast majority of somata in the VCN were FMRP+ (Fig. 3B). Here, nearly all globular bushy cells (GBC) are FMRP+ (95%, Fig. 5a) and the cell bodies of these neurons measured 451 ± 18 μm^2 (Figs. 4B and 5C). There were insufficient FMRP-immunonegative GBCs for statistical testing. In GBC, FMRP+ dendrites could be followed out to secondary dendritic branches (Fig. 4B, arrowheads). In the GBC region, there was also heavy FMRP+ labeling in the neuropil, which was absent from the layers of the DCN and OC (Fig. 4B).

In the rostral VCN (rVCN), the majority of spherical bushy cells (SBC) and stellate neurons were FMRP+ (Fig. 4C, asterisk and arrowhead, respectively). Specifically, 85% of SBC and 68% of stellate neurons were FMRP+ (Fig. 5A). There were no statistical differences in cell body size between FMRP+ and FMRP-immunonegative SBC or stellate neurons (SBC: 278 ± 10 μm^2 vs. 307 ± 21 μm^2; stellate: 265 ± 15 μm^2 compared to 278 ± 26 μm^2, Mann–Whitney, $p > .05$; Fig. 5C). However, FMRP+ SBC were significantly more round than FMRP-immunonegative SBC (.77 ± .008 vs. .72 ± .02, Mann–Whitney, $p = .001$, Fig. 5B). Additionally, throughout the VCN there were occasional small, fusiform neurons (average soma size = 163 ± 18 μm^2). Only 42% of these fusiform neurons were FMRP+ and we found no statistical difference in cell body size between FMRP+ and FMRP-immunonegative fusiform neurons (Fig. 5C). In the SBC region, there was also heavy FMRP labeling in the neuropil (Fig. 4C).

SOC

As in the VCN, the majority of SOC neurons were FMRP+ (Fig. 6). Within the MSO, the majority of neuronal cell bodies were FMRP+ and we estimated that 40% of all FMRP+ neurons in the human SOC are within the MSO. In MSO neurons, FMRP immunolabeling extended from the somata to reach primary and secondary dendritic arbors. Medial and lateral to the MSO cell column there was a halo which included dense tangles of FMRP+ dendritic profiles (black dashed line in Fig. 6 and black arrowheads in 7A). Closer examination of this territory revealed that many of these profiles could be traced back to a soma in the MSO (Fig. 7A, B). The MSO cell column was about 200-μm wide medial–laterally. At the mid-anteroposterior level of the cell column, FMRP+ dendritic profiles extended both medial and laterally up to 450 μm from MSO somata. In the specimens examined in this study, 83% of all MSO neurons were FMRP+ and we found no difference in cross sectional area between FMRP+ MSO somata and FMRP-immunonegative neurons (250 ± 6 μm^2 compared to 237 ± 26 μm^2, Mann–Whitney, $p = .08$, Fig. 11A). We examined FMRP-immunoreactivity in subpopulations of MSO neurons and found that 88% of fusiform, 79% of stellate neurons and 88% of round

Author's personal copy

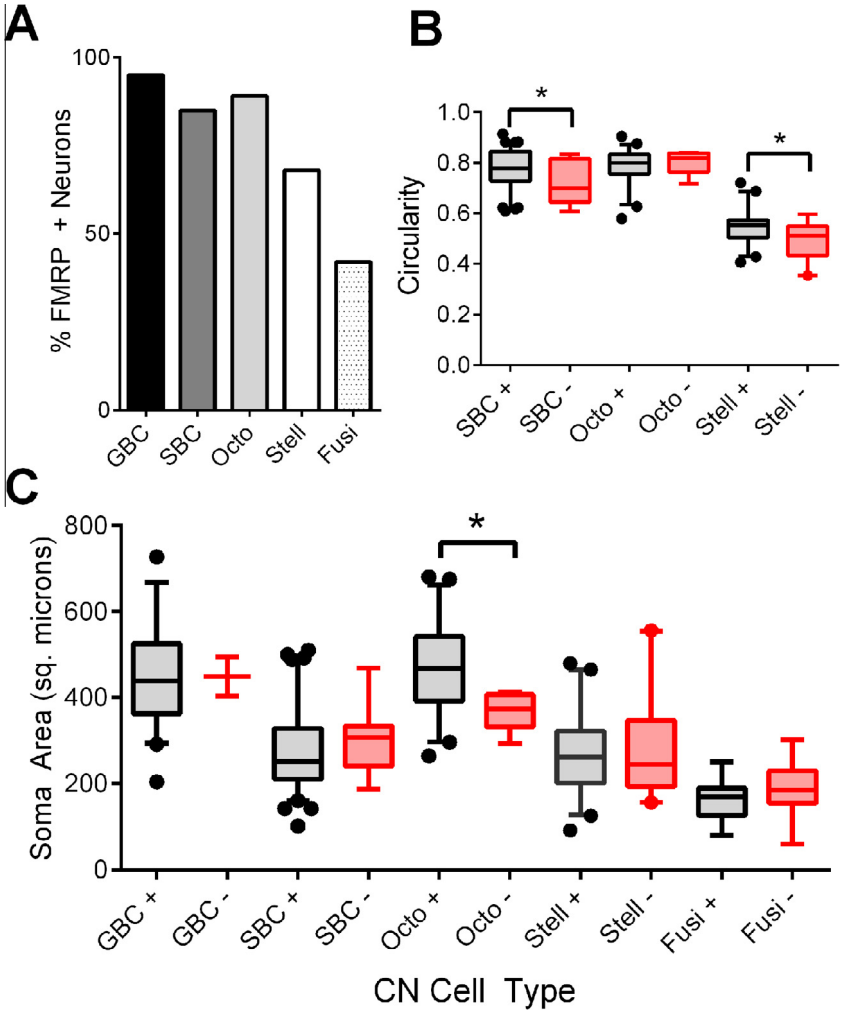

Fig. 5. Quantification of FMRP in the VCN. In A, the percentage of VCN cell types that are FMRP + is shown. Most neurons are FMRP + except for fusiform neurons of which less than 50% are FMRP + . Shown in B is a plot of circularity for each neuronal subpopulation. For SBC and stellate cells, FMRP + somata were more round when compared to FMRP-immunonegative cells. Shown in C is the cell body area by VCN cell type. FMRP + octopus cells had significantly larger cell bodies when compared to FMRP-immunonegative cells. In B and C the box plots are of 5–95th percentile.

MSO neurons were FMRP + . We found no statistical difference in cell body size between FMRP + and FMRP-immunonegative subpopulations (Fig. 11A; Mann–Whitney, fusiform $p = .45$; stellate $p = .26$; round $p = .34$). Additionally, we considered that FMRP-immunonegative MSO neurons might comprise a topographical subset of MSO neurons. However, we found no correlation of x and y coordinates of FMRP-immunonegative neurons (Pearson, $r^2 = .01$; $p = .19$) and no difference in the anterior–posterior location in the MSO cell column (Fig. 8; Mann–Whitney, $p = .58$). Finally, we examined colocalization of FMRP and the Kv3.1b potassium channel in human MSO neurons. We found notable overlap of FMRP and Kv3.1b immunolabeling in somata (asterisks in Fig. 9A–C) and dendrites (arrowheads in Fig. 9D). Additionally, there were abundant FMRP + axon profiles in the vicinity of the MSO (open arrowheads).

Within the lateral superior olive (LSO), the majority of neurons were FMRP + (87%; Fig. 10A). Of all LSO neurons, 33% were FMRP + stellate neurons and 58% were FMRP + round neurons. However, we found no differences in soma size between fusiform, stellate or round cell populations (Fig. 11B; Mann–Whitney, p all $> .05$). Additionally in the LSO, FMRP-immunolabeling extended from the soma into primary dendrites and heavy FMRP-immunoreactivity was observed in the neuropil of the LSO. This heavy pattern of neuropil labeling was not identified in any of the other SOC nuclei (Figs. 6 and 10A).

Within the superior paraolivary nucleus (SPON), the majority of neurons were FRMP + (83%; Fig. 10B). Of all SPON neurons, 34% were FMRP + stellate neurons and 52% were FMRP + round neurons. FMRP + stellate neurons were generally larger than FMRP-immunonegative stellate neurons (Fig. 11D; 256 ± 23 vs. 162 ± 14 μm^2) but this difference did not reach statistical significance (Mann–Whitney, $p = .10$). There were no differences between fusiform and round cell populations (Mann–Whitney, $p > .05$; Fig. 11D).

Author's personal copy

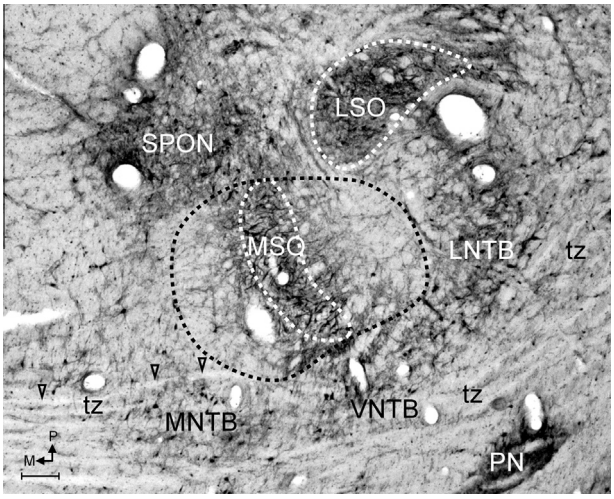

Fig. 6. Distribution of FMRP in the SOC. This figure shows a transverse section through the middle third of the SOC immunolabeled for FMRP. FMRP is widely expressed in SOC neurons but the pattern of labeling the neuropil varies. Neuropil labeling is heaviest in the LSO (white dashed line) and very light on either side of the MSO cell column (white dashed line), a region occupied by FMRP+ MSO dendrites (black dashed line). FMRP-immunolabeling is largely absent from axons in the trapezoid body (tz; arrowheads). Scale bar = 200 μm.

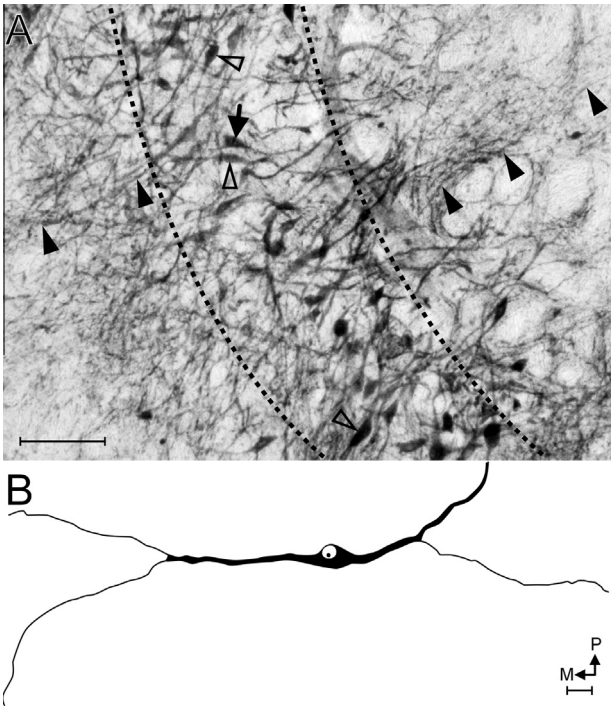

Fig. 7. FMRP is localized to MSO cell bodies and dendrites. Shown in A is a field of the MSO from a mid-rostral caudal level of the nucleus. The dashed line indicates the boundaries of the MSO cell column. The majority of MSO neurons are FMRP+. FMRP+ fusiform (open arrowheads) and stellate neurons (arrow) are demonstrated. FMRP+ dendritic profiles are found in the fields medial and lateral to the MSO cell column (arrowheads). Scale bar = 100 μm. Shown in B is a tracing of an FMRP+ MSO neuron from the caudal aspect of the nucleus. Note that FMRP-immunolabeling extends from the soma into dendrites out to secondary branches. Scale bar = 20 μm.

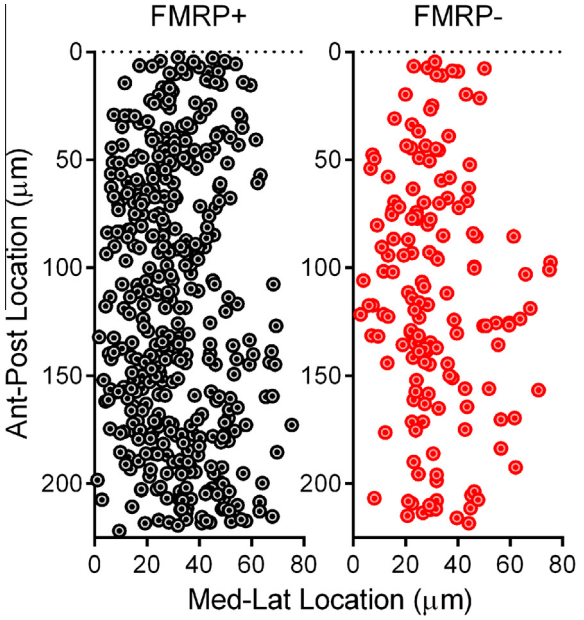

Fig. 8. FMRP-immunonegative MSO neurons have no topographic preference. Both A (FMRP+) and B (FMRP-immunonegative) show normalized plots, based on *x* and *y* coordinates, of MSO neurons from the middle 1/3 of the nucleus. Note that FMRP-immunonegative neurons span the entire anterior–posterior extent of the nucleus and show no topographic preference.

In the remaining SOC nuclei (medial nucleus of the trapezoid body (MNTB), ventral nucleus of the trapezoid body (VNTB) and lateral nucleus of the trapezoid body (LNTB); Fig. 6), we again found that the majority of neurons were FMRP+ (89%, 82% and 87%, respectively) and 94% of MNTB round/principal neurons and 85% of LNTB stellate neurons were FMRP+. As in other nuclei, FMRP-immunolabeling extended from the cell body into primary dendrites. There were no differences in cell body size between FMRP+ and FMRP negative neurons in these nuclei (Mann–Whitney, $p > .05$; Fig. 11C–F). Of all MNTB neurons, 76% were FMRP+ round cells and 63% of LNTB neurons were FMRP+ round neurons (Fig. 9C). Finally, we estimated that approximately 21% of all SOC FMRP+ neurons are localized to the LNTB.

DISCUSSION

To the best of the authors' knowledge, this is the first quantitative investigation of FMRP-immunolabeling in the human brainstem and the first characterization of FMRP+ neurons in the human cochlear nucleus and SOC. We have identified FMRP+ neurons in each of the brainstem nuclei we investigated, but the proportion varied considerably by nucleus. Specifically, we found that nearly 85% of FN neurons but only about 13% of neurons in the principal nucleus of the IO were FMRP+. We interpret these observations to indicate that FMRP is widely expressed but not ubiquitous in the human brainstem and that FMRP may function more prominently in some nuclei (FN, MSO) than others (IO). Additionally, the neuronal populations which abundantly

Author's personal copy

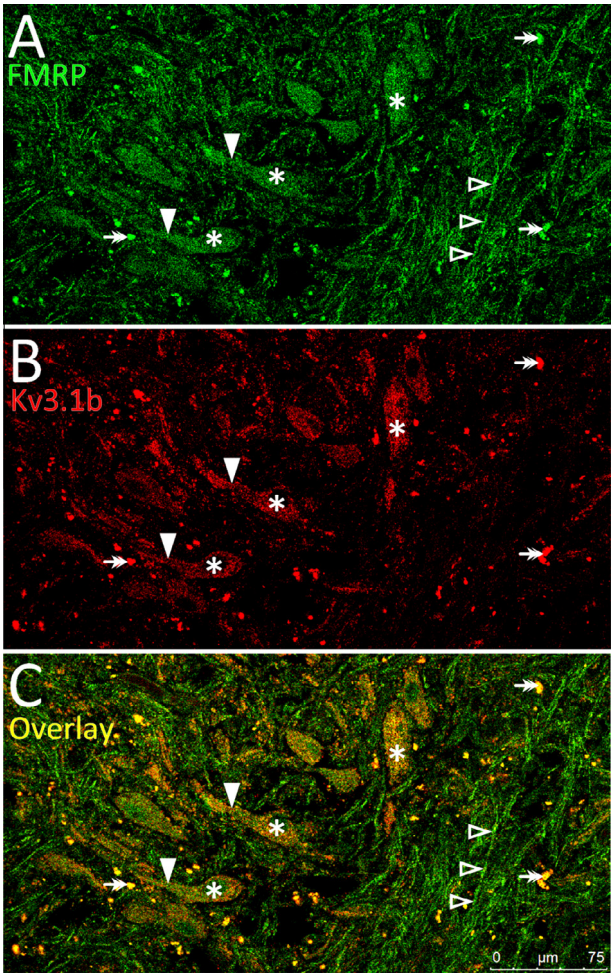

Fig. 9. FMRP colocalizes with Kv3.1b in the human MSO. Shown in A–C is a region of the MSO, immunolabeled for FMRP (A) and Kv3.1b (B). Three FMRP+ MSO neurons are indicated (A, empty arrowheads). In B, neuronal cell bodies (empty arrowheads) and punctate profiles (white arrowheads) are Kv3.1b-immunoreactive. Both A, B are overlaid in C; regions of colocalization are indicated in yellow. A lipofuscin artifact is indicated by the double arrow. Scale bar = 30 µm. Shown in D is a higher magnification view of an MSO neuron (soma indicated by asterisk; primary dendrites indicated by open arrowheads) immunolabeled for FMRP and Kv3.1b. Regions of colocalization in the cell body and dendrites are indicated in yellow. A lipofuscin artifact is indicated by the double arrow. Scale bar = 30 µm.

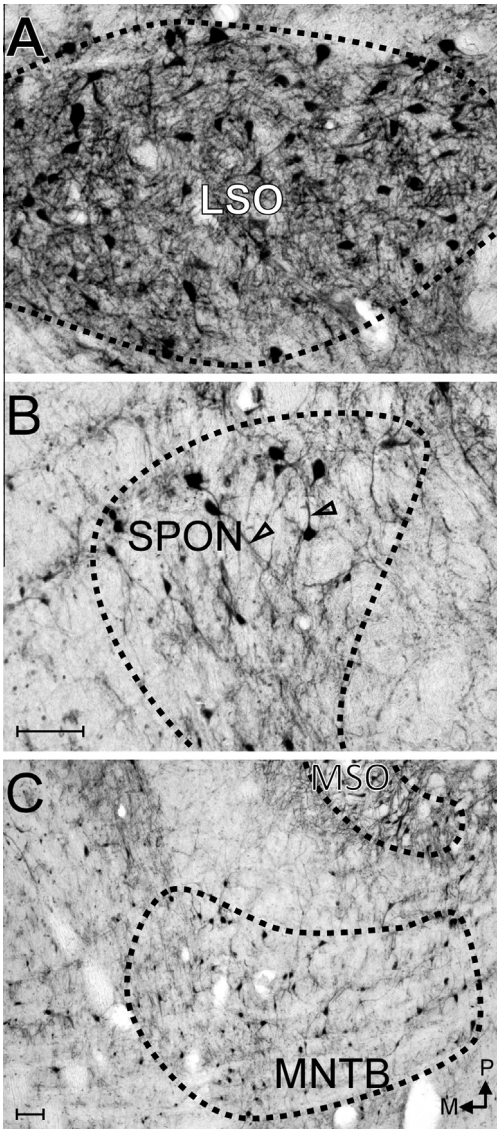

Fig. 10. FMRP is abundant in the SOC nuclei. Shown in A is FMRP-immunolabeling in the LSO. The majority of LSO neurons are FMRP+ and there is a high density of FMRP-immunoreactive linear profiles, which we interpret as dendrites arising from LSO neurons. Shown in B is FMRP-immunolabeling in the SPON. The majority of SPON neurons are FMRP+ and FMRP-immunolabeled dendrites are seen to emerge from SPON cell bodies. The neuropil labeling is relatively light in the SPON. Scale bar = 100 µm (B); A, B are at the same scale. Shown in C is FMRP-immunolabeling in the MNTB. Again, the majority of MNTB neurons are FMRP+ and the neuropil labeling is generally light. Scale bar = 100 µm (C).

express FMRP are likely to be more severely impacted in FXS or Fmr1 KO animals that those with minimal FMRP expression. Finally, the reader should be reminded that the subjects used in this investigation ranged in age from 57 to 96 years. We are open to the possibility that FMRP expression patterns may change with age and that these patterns may be markedly different in human neonatal populations. Regardless, FMRP is abundantly expressed in the auditory brainstem of the 57–96-year-old age group and likely plays an important functional role within these neuronal populations.

Within the cochlear nuclei and SOC, we found the majority of neurons and neuronal subtypes to be FMRP+. In the human DCN, we identified a group of large stellate/fusiform neurons between the molecular and granule layers (Wagoner and Kulesza, 2009; present study), the majority of which are FMRP+. We believe these stellate/fusiform neurons to be equivalent to pyramidal or fusiform neurons described previously in the DCN and further, that this population is a major source of DCN output to the inferior colliculus (Oertel and Golding, 1997; Oertel and Young, 2004). Since the DCN is known to integrate auditory and non-auditory information and relay information to the inferior colliculus, our findings suggest that FMRP plays an important role in this function. In the human VCN, we found that nearly all GBC and the vast majority of SBC, stellate and octopus cells

Author's personal copy

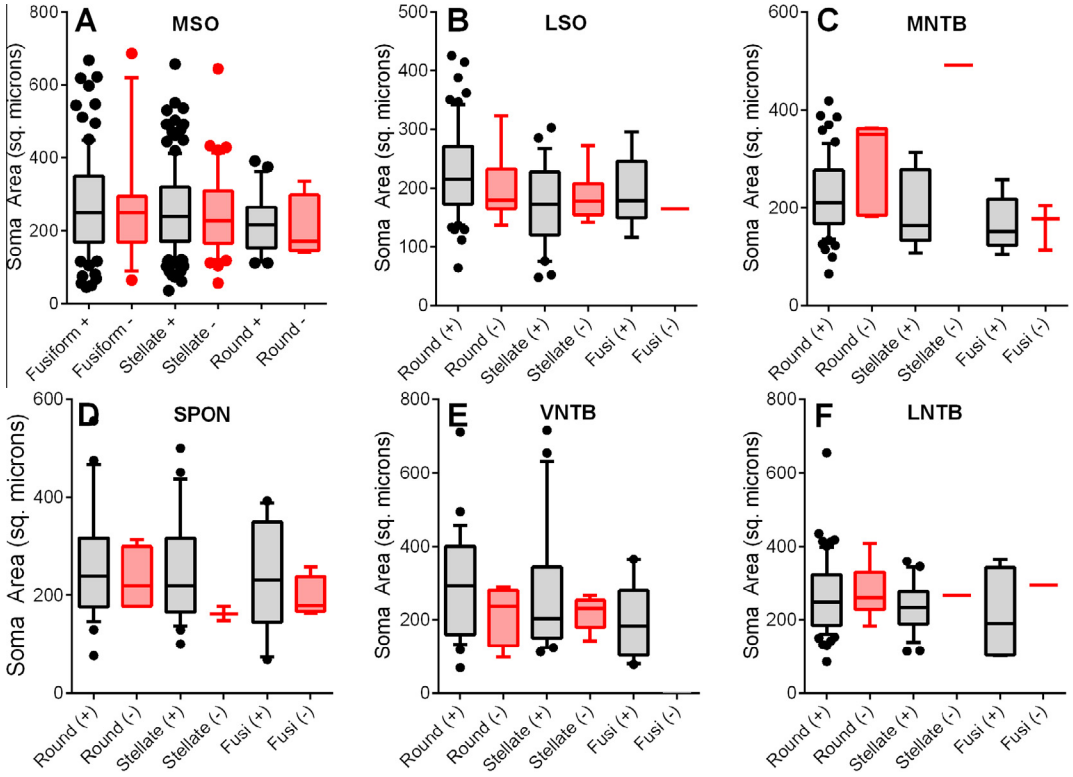

Fig. 11. Quantification of FMRP in the SOC. Shown in A–F are box plots of cell body area by SOC nucleus, cell body morphology (fusiform, stellate and round) and FMRP-immunoreactivity (FMRP + in black, FMRP-immunonegative in red). In the SPON, FMRP + somata were significantly larger than FMRP-immunonegative somata. All box pots are of 10–90th percentile. (For interpretation of the references to color in this figure legend, the reader is referred to the web version of this article.)

were FMRP + . Additionally, we found that FMRP + SBC had more circular cell bodies compared to FMRP-immunonegative SBC. Cell body shape and dendritic architecture are interdependent morphometric features and a less circular (i.e. more irregular) cell body contour results when 2 or more primary dendrites originate from the soma. We suggest that FMRP-immunonegative SBC may be distinguishable by multiple primary dendrites (see Figs. 3–5 in Cant, 1992). We also found that FMRP + octopus cells had larger somata compared to FMRP-immunonegative octopus cells. If a larger soma is required to support further-reaching or more elaborate dendritic arbors and/or axonal projections (Friede, 1963; Kulesza et al., 2011), FMRP + octopus cells might be distinguished from FMRP-immunonegative octopus cells by the complexity of dendritic arbors, axonal length and/or size of the axons terminal field. Because of the abundance of FMRP in the VCN, we suggest that FMRP plays an important role in processing temporal information and is essential for the relay of precisely timed action potentials to the SOC, nuclei of the lateral lemniscus and inferior colliculus. Within the SOC, we found the majority of LSO neurons to be FMRP + and within this nucleus we encountered heavy neuropil labeling, which was also observed in the cochlear nucleus. In these regions, FMRP may be localized to presynaptic sites (Christie et al., 2009) and within astrocytes (Pacey and Doering, 2007; Higashimori et al., 2013). The vast majority of MSO neurons were FMRP + and FMRP-immunolabeling in these neurons extended from the soma out to secondary dendritic branches. FMRP-immunonegative MSO neurons were not confined to a specific region of the nucleus, but were found throughout the MSO contour. Furthermore, we observed colocalization of FMRP and the high-voltage-activated potassium channel Kv3.1b in human MSO neurons. Colocalization of FMRP and Kv3.1b suggests the possibility that in the human MSO, FMRP may regulate Kv3.1b translation in a tonotopic fashion as in mouse (Strumbos et al., 2010). Overall, we have found that FMRP is abundantly expressed in neuronal somata and dendritic profiles. This localization suggests that FMRP plays an important role in normal function and dendritic processing in the DCN, VCN and SOC. Furthermore, we anticipate that with loss of FMRP function (as in FXS), these auditory brainstem centers will demonstrate significant errors in processing temporal features and localization of complex sounds.

Hypersensitivity to auditory and visual stimuli is a cardinal feature of FXS (Miller et al., 1999) and auditory-processing difficulties are well documented in FXS. Specifically, FXS is associated with increased amplitude of early cortical auditory-evoked potentials (St Clair et al., 1987; Rojas et al., 2001; Castrén et al., 2003; Van der Molen et al., 2012a) and patients with FXS are less accurate, have more false alarms and delayed reaction time in visual and auditory tasks (Van der Molen et al., 2012b). Further, FXS patients are known to exhibit language delay (Brady et al., 2006), hypersensitivity to

Author's personal copy

auditory stimulation (Van der Molen et al., 2012a), altered brain activation patterns during auditory discrimination tasks (Hall et al., 2009), weak auditory-processing skills and characteristic cluttering of speech (Hanson et al., 1986), normal latency of early cortical responses but increased amplitude and reduced lateralization (Knoth and Lippé, 2012). Fmr1 KO mice also exhibit auditory hypersensitivity and are susceptible to fatal sound-induced seizures (Chen and Toth, 2001; Nielsen et al., 2002). Single-unit recordings from the auditory cortex of Fmr1 KO mice (Rotschafer and Razak, 2013) reveal broader frequency receptive fields, pure tone stimuli elicit significantly more spikes and there is more variability in first-spike latency compared to control animals. Additionally, in an animal model of FXS, FMRP has been shown to play an essential role in maturation of the acoustic startle response (Yun et al., 2006).

To restate our major findings, we have demonstrated abundant neuronal FMRP-immunolabeling in the human cochlear nucleus and SOC, structures which play essential roles in processing temporal features of speech, sound source localization and descending modulation of the cochlea. Even though much of the literature to date has focused on cortical aspects of FMRP function, we suggest that auditory dysfunction in FXS may arise, at least in part, from timing errors in the CN and SOC. Additionally, it should be noted that auditory brainstem responses and hearing thresholds in young males with FXS do not differ significantly from controls (Roberts et al., 2005). We propose that the errors in temporal processing that are likely present in the FMRP-deficient CN and MSO cannot be detected on routine audiological screening tests, but become evident in vocalization and speech-based tasks.

Processing of interaural time differences (ITDs) in the MSO requires precisely timed convergence and segregation of both excitatory inputs from the CN and inhibitory inputs from within the SOC (Smith et al., 2000; Brand et al., 2002; Pecka et al., 2008; Couchman et al., 2012). Inappropriate group 1 mGluR signaling is proposed to contribute to the pathophysiological changes in FXS (Bear et al., 2004). Additionally, in Fmr1 KO mice, there is increased seizure activity and reduced expression of $GABA_A$ receptors/subunits (Miyashiro et al., 2003; El Idrissi et al., 2005; Gantois et al., 2006; D'Hulst et al., 2006) and abnormal GAD65/67 expression (El Idrissi et al., 2005; Olmos-Serrano et al., 2010). It is possible then that in FXS, there is a disruption of the delicate balance of excitation and inhibition required for ITD coding in the MSO and this may lead to significant processing errors (Brand et al., 2002; Hassfurth et al., 2010; Grothe and Koch, 2011).

CONFLICT OF INTEREST

The authors declare that there are no conflicts of interest.

Acknowledgments—This work was supported in part by a grant from the Lake Erie Consortium for Osteopathic Medical Training. The authors would like to thank Jerome McGraw, Kristen Ruby and George Grignol for technical assistance.

REFERENCES

Akins MR, Berk-Rauch HE, Fallon JR (2009) Presynaptic translation: stepping out of the postsynaptic shadow. Front Neural Circuits 3:17.

Akins MR, Leblanc HF, Stackpole EE, Chyung E, Fallon JR (2012) Systematic mapping of fragile X granules in the mouse brain reveals a potential role for presynaptic FMRP in sensorimotor functions. J Comp Neurol 520(16):3687–3706.

Bassell GJ, Warren ST (2008) Fragile X syndrome: loss of local mRNA regulation alters synaptic development and function. Neuron 60:201–214.

Bear MF, Huber KM, Warren ST (2004) The mGluR theory of fragile X mental retardation. Trends Neurosci 27(7):370–377.

Berry-Kravis E (2002) Epilepsy in fragile X syndrome. Dev Med Child Neurol 44(11):724–728.

Brady N, Skinner D, Roberts J, Hennon E (2006) Communication in young children with fragile X syndrome: a qualitative study of mothers' perspectives. Am J Speech Lang Pathol 15(4):353–364.

Brand A, Behrend O, Marquardt T, McAlpine D, Grothe B (2002) Precise inhibition is essential for microsecond interaural time difference coding. Nature 417(6888):543–547.

Braun K, Segal M (2000) FMRP involvement in formation of synapses among cultured hippocampal neurons. Cereb Cortex 10(10):1045–1052.

Brown MR, Kronengold J, Gazula VR, Chen Y, Strumbos JG, Sigworth FJ, Navaratnam D, Kaczmarek LK (2010) Fragile X mental retardation protein controls gating of the sodium-activated potassium channel Slack. Nat Neurosci 13(7):819–821.

Cant NB (1992) The cochlear nucleus: neuronal types and their synaptic organization. In: Webster DB, Popper AN, Fay RR, editors. The mammalian auditory pathway: neuroanatomy. Berlin: Springer-Verlag. p. 66–116.

Castrén M, Pääkkönen A, Tarkka IM, Ryynänen M, Partanen J (2003) Augmentation of auditory N1 in children with fragile X syndrome. Brain Topogr 15(3):165–171.

Castren M, Tervonen T, Karkkainen V, Heinonen S, Castren E, Larsson K, Bakker CE, Oostra BA, Akerman K (2005) Altered differentiation of neural stemcells in fragile x syndrome. Proc Natl Acad Sci U S A 102:17834–17839.

Chen L, Toth M (2001) Fragile X mice develop sensory hyperactivity to auditory stimuli. Neuroscience 103:1043–1050.

Christie SB, Akins MR, Schwob JE, Fallon JR (2009) The FXG: a presynaptic fragile x granule expressed in a subset of developing brain circuits. J Neurosci 29:1514–1524.

Comery TA, Harris JB, Willems PJ, Oostra BA, Irwin SA, Weiler IJ, Greenough WT (1997) Abnormal dendritic spines in fragile X knockout mice: maturation and pruning deficits. Proc Natl Acad Sci U S A 94(10):5401–5404.

Cornish K, Turk J, Hagerman R (2008) The fragile X continuum: new advances and perspectives. J Intellect Disabil Res 52(Pt 6): 469–482.

Couchman K, Grothe B, Felmy F (2012) Functional localization of neurotransmitter receptors and synaptic inputs to mature neurons of the medial superior olive. J Neurophysiol 107(4):1186–1198.

D'Hulst C, De Geest N, Reeve SP, Van Dam D, De Deyn PP, Hassan BA, Kooy RF (2006) Decreased expression of the GABAA receptor in fragile X syndrome. Brain Res 1121(1):238–245.

Deng PY, Rotman Z, Blundon JA, Cho Y, Cui J, Cavalli V, Zakharenko SS, Klyachko VA (2013) FMRP regulates neurotransmitter release and synaptic information transmission by modulating action potential duration via BK channels. Neuron 77(4):696–711.

Devys D, Lutz Y, Rouyer N, Bellocq JP, Mandel JL (1993) The FMR1 protein is cytoplasmic, most abundant in neurons and appears normal in carriers of fragile x permutation. Nat Genet 4:335–340.

El Idrissi A, Ding XH, Scalia J, Trenkner E, Brown WT, Dobkin C (2005) Decreased GABA(A) receptor expression in the seizure-prone fragile X mouse. Neurosci Lett 377(3):141–146.

Eliez S, Blasey CM, Freund LS, Hastie T, Reiss AL (2001) Brain anatomy, gender and IQ in children and adolescents with fragile X syndrome. Brain 124(Pt 8):1610–1618.

Author's personal copy

Feng Y, Gutekunst CA, Eberhart DE, Yi H, Warren ST, Hersch SM (1997) Fragile X mental retardation protein: nucleocytoplasmic shuttling and association with somatodendritic ribosomes. J Neurosci 17(5):1539–1547.
Friede RL (1963) The relationship of body size, nerve cell size, axon length, and glial density in the cerebellum. Proc Natl Acad Sci U S A 49:187–193.
Galvez R, Gopal AR, Greenough WT (2003) Somatosensory cortical barrel dendritic abnormalities in a mouse model of the fragile X mental retardation syndrome. Brain Res 971(1):83–89.
Galvez R, Smith RL, Greenough WT (2005) Olfactory bulb mitral cell dendritic pruning abnormalities in a mouse model of the Fragile-X mental retardation syndrome: further support for FMRP's involvement in dendritic development. Brain Res Dev Brain Res 157(2):214–216.
Gantois I, Vandesompele J, Speleman F, Reyniers E, D'Hooge R, Severijnen LA, Willemsen R, Tassone F, Kooy RF (2006) Expression profiling suggests underexpression of the GABA(A) receptor subunit delta in the fragile X knockout mouse model. Neurobiol Dis 21(2):346–357.
Grothe B, Koch U (2011) Dynamics of binaural processing in the mammalian sound localization pathway – the role of GABA(B) receptors. Hear Res 279(1–2):43–50.
Hagerman RJ, Berry-Kravis E, Kaufmann WE, Ono MY, Tartaglia N, Lachiewicz A, Kronk R, Delahunty C, Hessl D, Visootsak J, Picker J, Gane L, Tranfaglia M (2009) Advances in the treatment of fragile X syndrome. Pediatrics 123(1):378–390.
Hall SS, Walter E, Sherman E, Hoeft F, Reiss AL (2009) The neural basis of auditory temporal discrimination in girls with fragile X syndrome. J Neurodev Disord 1(1):91–99.
Hanson DM, Jackson 3rd AW, Hagerman RJ (1986) Speech disturbances (cluttering) in mildly impaired males with the Martin-Bell/fragile X syndrome. Am J Med Genet 23(1–2):195–206.
Harris JC (2011) Autism spectrum disorders in neurogenic syndromes: phenocopies of Autism. In: Adam A, editor. Textbook of autism spectrum disorders. Washington, DC: American Psychiatric Publishing, Inc.
Hassfurth B, Grothe B, Koch U (2010) The mammalian interaural time difference detection circuit is differentially controlled by GABAB receptors during development. J Neurosci 30(29):9715–9727.
Hatton DD, Sideris J, Skinner M, Mankowski J, Bailey Jr DB, Roberts J, Mirrett P (2006) Autistic behavior in children with fragile X syndrome: prevalence, stability, and the impact of FMRP. Am J Med Genet 140:1804–1813.
Higashimori H, Morel L, Huth J, Lindemann L, Dulla C, Taylor A, Freeman M, Yang Y (2013) Astroglial FMRP-dependent translational down-regulation of mGluR5 underlies glutamate transporter GLT1 dysregulation in the fragile X mouse. Hum Mol Genet 22(10):2041–2054.
Hinds HL, Ashley CT, Sutcliffe JS, Nelson DL, Warren ST, Housman DE, Schalling M (1993) Tissue specific expression of FMR-1 provides evidence for a functional role in fragile X syndrome. Nat Genet 3:38–43.
Hinton VJ, Brown WT, Wisniewski K, Rudelli RD (1991) Analysis of neocortex in three males with the fragile X syndrome. Am J Med Genet 41(3):289–294.
Hoeft F, Carter JC, Lightbody AA, Cody Hazlett H, Piven J, Reiss AL (2010) Region-specific alterations in brain development in one- to three-year-old boys with fragile X syndrome. Proc Natl Acad Sci U S A 107(20):9335–9339.
Irwin SA, Galvez R, Greenough WT (2000) Dendritic spine structural anomalies in fragile-x syndrome. Nat Rev Neurosci 6:376–387.
Jacobs S, Cheng C, Doering LC (2012) Probing astrocyte function in fragile X syndrome. Results Probl Cell Differ 54:15–31.
Kates WR, Abrams MT, Kaufmann WE, Breiter SN, Reiss AL (1997) Reliability and validity of MRI measurement of the amygdala and hippocampus in children with fragile X syndrome. Psychiatry Res 75(1):31–48.
Klemmer P, Meredith RM, Holmgren CD, Klychnikov OI, Stahl-Zeng J, Loos M, van der Schors RC, Wortel J, de Wit H, Spijker S, Rotaru DC, Mansvelder HD, Smit AB, Li KW (2011) Proteomics, ultrastructure, and physiology of hippocampal synapses in a fragile X syndrome mouse model reveal presynaptic phenotype. J Biol Chem 286(29):25495–25504.
Knoth IS, Lippé S (2012) Event-related potential alterations in fragile X syndrome. Front Hum Neurosci 6:264.
Kulesza Jr RJ (2007) Cytoarchitecture of the human superior olivary complex: medial and lateral superior olive. Hear Res 225(1–2):80–90.
Kulesza Jr RJ (2008) Cytoarchitecture of the human superior olivary complex: nuclei of the trapezoid body and posterior tier. Hear Res 241(1–2):52–63.
Kulesza Jr RJ (2013) Characterization of human auditory brainstem circuits by calcium binding protein immunohistochemistry. Neuroscience 258:318–331.
Kulesza RJ, Mangunay K (2008) Morphological features of the medial superior olive in autism. Brain Res 1200:132–137.
Kulesza Jr RJ, Lukose R, Stevens LV (2011) Malformation of the human superior olive in autistic spectrum disorders. Brain Res 1367:360–371.
Li J, Pelletier MR, Perez Velazquez JL, Carlen PL (2002) Reduced cortical synaptic plasticity and GluR1 expression associated with fragile X mental retardation protein deficiency. Mol Cell Neurosci 19(2):138–151.
Miller LJ, McIntosh DN, McGrath J, Shyu V, Lampe M, Taylor AK, Tassone F, Neitzel K, Stackhouse T, Hagerman RJ (1999) Electrodermal responses to sensory stimuli in individuals with fragile X syndrome: a preliminary report. Am J Med Genet. 83(4):268–279.
Miyashiro KY, Beckel-Mitchener A, Purk TP, Becker KG, Barret T, Liu L, Carbonetto S, Weiler IJ, Greenough WT, Eberwine J (2003) RNA cargoes associating with FMRP reveal deficits in cellular functioning in Fmr1 null mice. Neuron 37(3):417–431.
Moore JK, Osen KK (1979) The cochlear nuclei in man. Am J Anat 154(3):393–418.
Mostofsky SH, Mazzocco MM, Aakalu G, Warsofsky IS, Denckla MB, Reiss AL (1998) Decreased cerebellar posterior vermis size in fragile X syndrome: correlation with neurocognitive performance. Neurology 50(1):121–130.
Nielsen DM, Derber WJ, McClellan DA, Crnic LS (2002) Alterations in the auditory startle response in Fmr1 targeted mutant mouse models of fragile X syndrome. Brain Res 927(1):8–17.
Nimchinsky EA, Oberlander AM, Svoboda K (2001) Abnormal development of dendritic spines in FMR1 knock-out mice. J Neurosci 21(14):5139–5146.
Oertel D, Golding NL (1997) Circuits of the dorsal cochlear nucleus. In: Syka, editor. Acoustical signal processing in the central auditory system. New York: Plenum Press.
Oertel D, Young ED (2004) What's a cerebellar circuit doing in the auditory system? Trends Neurosci 27(2):104–110.
Olmos-Serrano JL, Paluszkiewicz SM, Martin BS, Kaufmann WE, Corbin JG, Huntsman MM (2010) Defective GABAergic neurotransmission and pharmacological rescue of neuronal hyperexcitability in the amygdala in a mouse model of fragile X syndrome. J Neurosci 30(29):9929–9938.
Osen KK (1969) Cytoarchitecture of the cochlear nuclei in the cat. J Comp Neurol 136(4):453–484.
Pacey LK, Doering LC (2007) Developmental expression of FMRP in the astrocyte lineage: implications for fragile X syndrome. Glia 55(15):1601–1609.
Pecka M, Brand A, Behrend O, Grothe B (2008) Interaural time difference processing in the mammalian medial superior olive: the role of glycinergic inhibition. J Neurosci 28(27):6914–6925.
Pfeiffer BE, Huber KM (2009) The state of synapses in fragile X syndrome. Neuroscientist 15(5):549–567.
Reiss AL, Abrams MT, Greenlaw R, Freund L, Denckla MB (1995) Neurodevelopmental effects of the FMR-1 full mutation in humans. Nat Med 1(2):159–167.
Roberts J, Hennon EA, Anderson K, Roush J, Gravel J, Skinner M, Misenheimer J, Reitz P (2005) Auditory brainstem responses in young males with Fragile X syndrome. J Speech Lang Hear Res 48(2):494–500.

Author's personal copy

Rogers SJ, Wehner DE, Hagerman R (2001) The behavioral phenotype in fragile X: symptoms of autism in very young children with fragile X syndrome, idiopathic autism, and other developmental disorders. J Dev Behav Pediatr 22(6):409–417.

Rojas DC, Benkers TL, Rogers SJ, Teale PD, Reite ML, Hagerman RJ (2001) Auditory evoked magnetic fields in adults with fragile X syndrome. NeuroReport 12(11):2573–2576.

Rotschafer S, Razak K (2013) Altered auditory processing in a mouse model of fragile X syndrome. Brain Res 1506:12–24.

Rudelli RD, Brown WT, Wisniewski K, Jenkins EC, Laure-Kamionowska M, Connell F, Wisniewski HM (1985) Adult fragile X syndrome. Clinico-neuropathologic findings. Acta Neuropathol 67(3–4):289–295.

Schmidt E, Wolski Jr TP, Kulesza Jr RJ (2010) Distribution of perineuronal nets in the human superior olivary complex. Hear Res 265(1–2):15–24.

Smith AJ, Owens S, Forsythe ID (2000) Characterisation of inhibitory and excitatory postsynaptic currents of the rat medial superior olive. J Physiol 529(Pt 3):681–698.

St Clair DM, Blackwood DH, Oliver CJ, Dickens P (1987) P3 abnormality in fragile X syndrome. Biol Psychiatry 22(3):303–312.

Standring S (2008) Gray's anatomy: the anatomical basis of clinical practice. 40th ed. Churchill Livingstone.

Strumbos JG, Brown MR, Kronengold J, Polley DB, Kaczmarek LK (2010) Fragile X mental retardation protein is required for rapid experience- dependent regulation of the potassium channel Kv3.1b. J Neurosci 30:10263–10271.

Thomas CC, Combe CL, Dyar KA, Inglis FM (2008) Modest alterations in patterns of motor neuron dendrite morphology in the Fmr1 knockout mouse model for fragile X. Int J Dev Neurosci 26(7):805–811.

Van der Molen MJ, Van der Molen MW, Ridderinkhof KR, Hamel BC, Curfs LM, Ramakers GJ (2012a) Auditory change detection in fragile X syndrome males: a brain potential study. Clin Neurophysiol 123:1309–1318.

Van der Molen MJ, Van der Molen MW, Ridderinkhof KR, Hamel BC, Curfs LM, Ramakers GJ (2012b) Auditory and visual cortical activity during selective attention in fragile x syndrome: a cascade of processing deficiencies. Clin Neurophysiol 123:720–729.

Verkerk AJ, Pieretti M, Sutcliffe JS, Fu YH, Kuhl DP, Pizzuti A, Reiner O, Richards S, Victoria MF, Zhang FP (1991) Identification of a gene (FMR-1) containing a CGG repeat coincident with a breakpoint cluster region exhibiting length variation in fragile X syndrome. Cell 65(5):905–914.

Wagoner JL, Kulesza Jr RJ (2009) Topographical and cellular distribution of perineuronal nets in the human cochlear nucleus. Hear Res 254(1–2):42–53.

Wang H, Ku L, Osterhout DJ, Li W, Ahmadian A, Liang Z, Feng Y (2004) Developmentally-programmed FMRP expression in oligodendrocytes: a potential role of FMRP in regulating translation in oligodendroglia progenitors. Hum Mol Genet 13(1):79–89.

Wang Y, Sakano H, Beebe K, Brown MR, de Laat R, Bothwell M, Kulesza Jr RJ, Rubel EW (2013) Intense and specialized dendritic localization of the fragile X mental retardation protein in binaural brainstem neurons – a comparative study in the alligator, chicken, gerbil, and human. J Comp Neurol.

Yin TC, Chan JC (1990) Interaural time sensitivity in medial superior olive of cat. J Neurophysiol 64(2):465–488.

Yun SW, Platholi J, Flaherty MS, Fu W, Kottmann AH, Toth M (2006) Fmrp is required for the establishment of the startle response during the critical period of auditory development. Brain Res 1110(1):159–165.

Zarnescu DC, Jin P, Betschinger J, Nakamoto M, Wang Y, Dockendorff TC, Feng Y, Jongens TA, Sisson JC, Knoblich JA, Warren ST, Moses K (2005) Fragile X protein functions with lgl and the par complex in flies and mice. Dev Cell 8(1):43–52.

Zhang Y, Brown MR, Hyland C, Chen Y, Kronengold J, Fleming MR, Kohn AB, Moroz LL, Kaczmarek LK (2012) Regulation of neuronal excitability by interaction of fragile X mental retardation protein with slack potassium channels. J Neurosci 32:15318–15327.

(Accepted 2 May 2014)
(Available online 15 May 2014)